Bioconjugate Chemistry

pubs.acs.org/bc Article

Compact, "Clickable" Quantum Dots Photoligated with Multifunctional Zwitterionic Polymers for Immunofluorescence and *In Vivo* Imaging

Wentao Wang, Erna A. van Niekerk, Yang Zhang, Liang Du, Xin Ji, Sisi Wang, James D. Baker, Kimberly Groeniger, Françisco M. Raymo, and Hedi Mattoussi*

Cite This: *Bioconjugate Chem.* 2020, 31, 1497−1509 Read Online

ACCESS | Metrics & More | Article Recommendations | Supporting Information

ABSTRACT: We detail the preparation of highly fluorescent quantum dots (QDs), surface-engineered with multifunctional polymer ligands that are compact and readily compatible with strain-promoted click conjugation, and the use of these nanocrystals in immunofluorescence and *in vivo* imaging. The ligand design combines the benefits of mixed coordination (i.e., thiol and imidazole) with zwitterion motifs, yielding sterically-stabilized QDs that present a controllable number of azide groups, for easy conjugation to biomolecules *via* the selective click chemistry. The polymer coating was characterized using NMR spectroscopy to extract estimates of the diffusion coefficient, hydrodynamic size, and ligand density. The azide-functionalized QDs were conjugated to anti-tropomyosin receptor kinase B antibody (α-TrkB) or to the brain-derived neurotrophic factor (BDNF). These conjugates were highly effective for labeling the tropomyosin receptor kinase B (TrkB) in pyramidal neurons within cortical tissue and for monitoring the BDNF induced activation of TrkB signaling in live neuronal cells. Finally, the polymer-coated QDs were applied for *in vivo* imaging of *Drosophila melanogaster* embryos, where the QDs remained highly fluorescent and colloidally stable, with no measurable cytotoxicity. These materials would be of great use in various imaging applications, where a small size, ease of conjugation, and great colloidal stability for *in vivo* studies are needed.

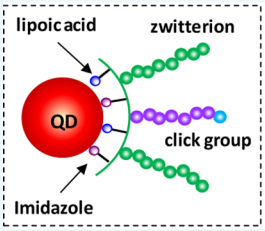

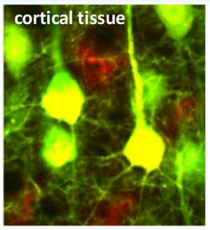

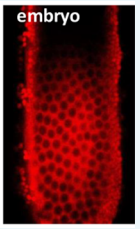

INTRODUCTION

Semiconductor quantum dots (QDs), such as core−shell CdSe/ZnS nanocrystals, exhibit unique size- and composition-dependent photophysical properties along with nanoscale dimensions that are comparable to those of biomolecules (e.g., proteins).[1−9] These features combined make them appealing for use as biological probes and diagnostic tools to investigate diverse biological processes at the single cell level.[8,10−19] However, using QDs in biology has been constrained by several limitations, including large hydrodynamic size, limited colloidal stability under physiological conditions, nonspecific interactions, and low targeting efficiency in biological fluids.[20−23] These properties are primarily influenced by the surface coating strategy utilized.

Ligand exchange is an effective approach for tailoring the QD surface properties; such strategy relies on the competitive displacement of the native hydrophobic molecules and their substitution with new bifunctional hydrophilic ligands. These ligands are typically composed of anchoring groups for coordination on the nanoparticle surfaces and hydrophilic motifs to promote steric stabilization in buffer media. Over the past two decades, a variety of coordinating ligands have been developed. Among these, multifunctional polymer ligands show advantageous features. Compared with molecular-scale ligands, polymers can display several anchoring groups per single ligand, allowing for binding onto the nanoparticle surface through multisite coordination.[24,25] Such enhanced interactions greatly reduce the rate of ligand desorption from the nanoparticle surface, thereby substantially improving the colloidal stability in a wide range of conditions. Moreover, polymers comprising distinct functionalities within the same structure can be readily prepared. This "all in one" design provides better control over the ligand stoichiometry as well as the nature of each installed module, allowing for careful tuning of the nanoparticle surface properties.

In earlier studies, polymer ligands appended with thiol anchors have been extensively exploited, since these groups exhibit strong affinity to QD surfaces.[24,26−28] However, thiol groups tend to negatively affect the fluorescence properties of QDs.[29,30] In addition, this mode of surface coordination can be weakened by oxidation of the thiols.[31] To overcome some of these drawbacks, imidazole-based polymer ligands have been

Received: March 26, 2020
Revised: April 24, 2020
Published: April 25, 2020

https://dx.doi.org/10.1021/acs.bioconjchem.0c00169
Bioconjugate Chem. 2020, 31, 1497−1509

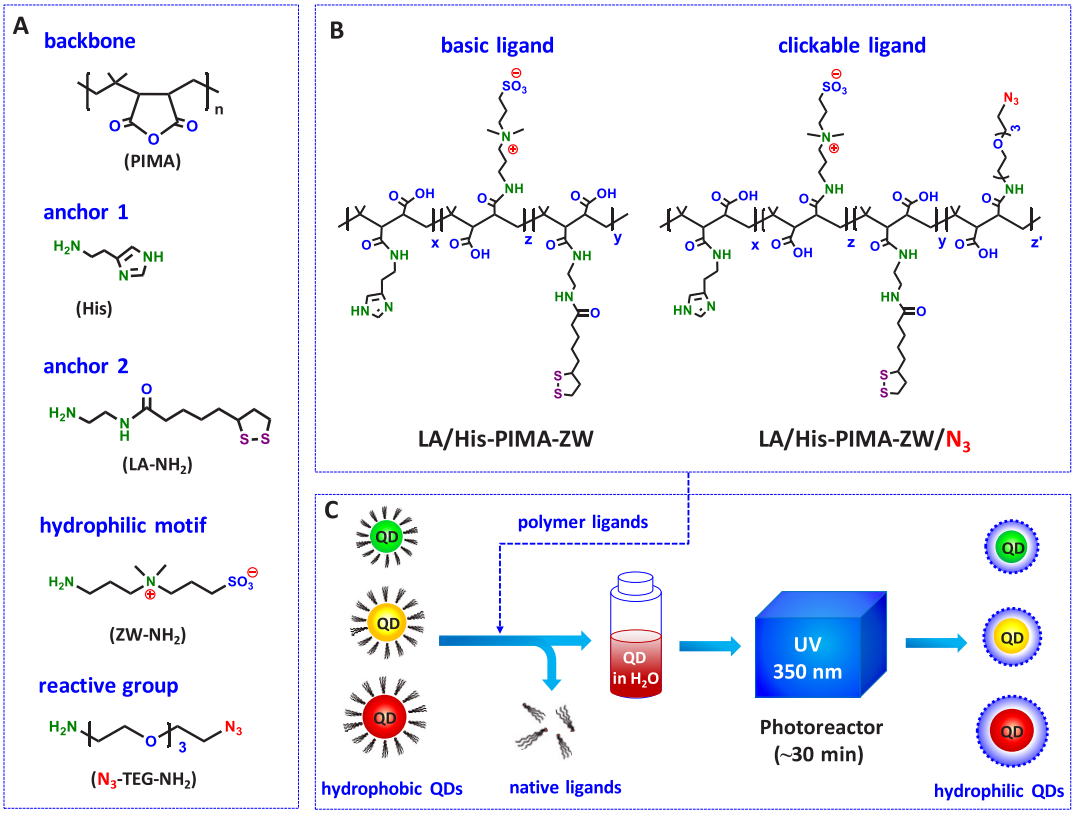

Figure 1. (A) Chemical structures of the building blocks used for the synthesis of the polymer ligands, including the central scaffold, PIMA; the hydrophilic moiety, ZW-NH_2; the anchoring groups, LA-NH_2 and histamine; and the functional group, N_3-TEG-NH_2. (B) Representative polymer ligands: LA/His-PIMA-ZW and LA/His-PIMA-ZW/N_3. (C) Schematics of the ligand exchange of QDs with the polymers mediated by UV irradiation.

proposed as an alternative to thiolated ones.[32−39] Imidazole is not affected by issues of photo-oxidation, and it can potentially enhance the QD fluorescence.[32,33,40] Nonetheless, the coordination strength of imidazoles is weaker than that of thiols, particularly in acidic conditions (pH < 6).[33] Building on these observations, our group explored the use of polymer ligands with mixed coordination where two types of anchoring groups, lipoic acid and imidazole, are combined within the same ligand structure to bind on the QDs.[45] This new design indeed exploits the benefits of the two anchors and synergistically addresses the issues of thiol oxidation and weaker binding of imidazole groups, if only one type of anchors is used.

The hydrophilic motif also plays a critical role in the ligand functions. It ensures the steric stabilization of nanoparticles in aqueous media and controls their interactions with biological systems.[41,42] The use of poly(ethylene glycol) (PEG) blocks as the hydrophilic motif in the ligand design has proved to be effective in improving colloidal stability while drastically reducing nonspecific protein absorption. We and others have designed a set of PEGylated polymer ligands for the surface functionalization of QDs, including the one with mixed coordination as described above.[26,32,36,43−45] However, to achieve good water affinity, high molecular weight PEG blocks are often used, which tends to increase the hydrodynamic size of the nanoparticles. Such a large size can negatively affect the efficiencies of QD-based sensors and can limit their ability to access confined regions, such as the synaptic regions in neuron cell cultures.[46,47] To reduce the hydrodynamic dimensions of the hydrophilic materials, ligands appended with zwitterion groups have been developed.[33,34,48−52] Given their molecular-scale, these groups yield compact coating and reduce the overall size of the nanocrystals. Nonetheless, synthesizing zwitterion-modified ligands and applying them in ligand exchange protocols is challenging, due to the very limited solubility of these groups in commonly used organic solvents.

In this study, we report the design of a set of polymer ligands that combine the benefits of zwitterions' small size with mixed coordination, to allow for easy functionalization of luminescent QDs and facilitate their application in biology. The ligands are prepared *via* the one-step nucleophilic addition reaction starting with poly(isobutylene-*alt*-maleic anhydride), PIMA, which yields a modular structure presenting multiple imidazole/lipoic acid anchors to promote strong coordination, several zwitterion moieties, and a few terminally reactive tetraethylene glycol blocks to guarantee biocompatibility and tunable surface reactivity of the QDs. Photoligation with these ligands provides QD dispersions with high fluorescence and excellent colloidal stability over a broad range of conditions. The polymer-coated QDs are characterized using several analytical tools including UV−visible absorption, fluorescence spectroscopy, Fourier transform infrared spectroscopy (FT-IR), and NMR spectroscopy. Introducing azide functions in the ligands has allowed conjugation of the QDs to anti-tropomyosin receptor kinase B antibody (α-TrkB) and to the brain-derived neurotrophic factor (BDNF), *via* strain-promoted click chemistry. This provided the means to visualize the distribution of TrkB in pyramidal neurons within cortical tissue and the activation of BDNF/TrkB signaling in live neuronal cells. The colloidal stability and cytotoxicity of the

https://dx.doi.org/10.1021/acs.bioconjchem.0c00169
Bioconjugate Chem. 2020, 31, 1497−1509

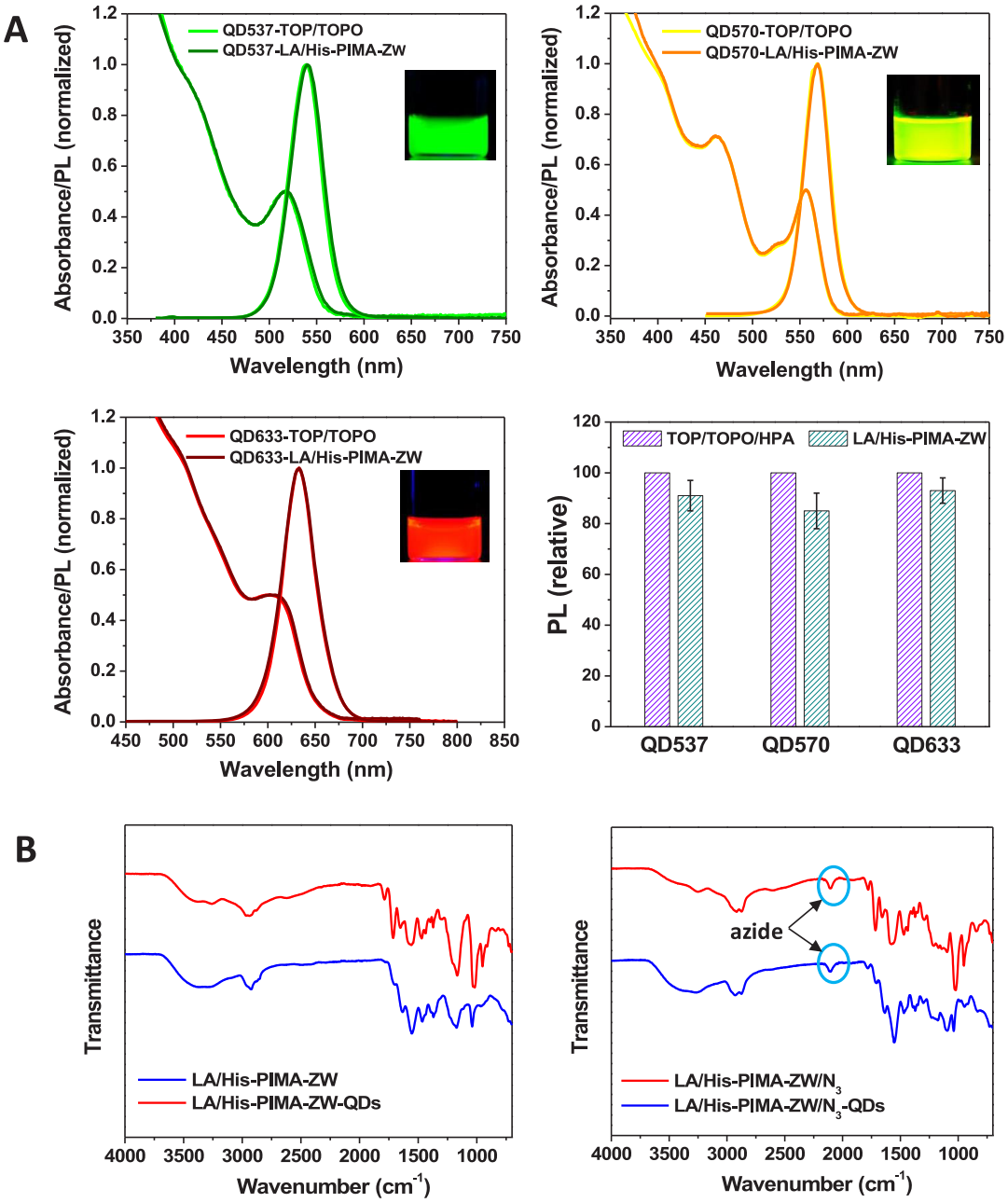

Figure 2. (A) Normalized absorption and fluorescence spectra collected from QD537, QD570, and QD633, before and after ligand exchange with LA/His-PIMA-ZW, along with the relative PL intensities of QDs ligated with LA/His-PIMA-ZW in water compared with the hydrophobic QDs in hexane; the same optical density was used for both sets. (B) FT-IR spectra collected from QDs ligated with LA/His-PIMA-ZW (left) and QDs ligated with LA/His-PIMA-ZW/N_3 (right), along with the corresponding pure polymer ligands.

polymer-coated QDs were evaluated by *in vivo* imaging of *Drosophila melanogaster* embryos.

RESULTS AND DISCUSSION

The zwitterionic polymer ligands with mixed coordination described in this report were inspired by ideas introduced in our previous works.[25,33,45,53] The synthetic route exploits the effectiveness of the one-step nucleophilic addition reaction between PIMA and H_2N-R nucleophiles, where a near 100% reaction efficiency is achieved without requiring coupling reagents.[45,54] These features simplify ligand purification and bode well for preparing zwitterion-rich polymers, given the stringent solubility of these groups in organic solvents. We reasoned that the ligand structure that combines mixed coordination with zwitterion groups can promote high affinity to the nanocrystals and enhance the photoluminescence (PL) properties of the QDs, while guaranteeing highly compact coating.[33] In addition, to introduce the azide groups without compromising the compactness of the coating, we selected H_2N-TEG-N_3 (using a tetraethylene glycol segment) as the nucleophile for the addition reaction. The stoichiometry of the coating ligand can be easily tuned by controlling the molar fraction of each functionality used with respect to that of the anhydride groups in the PIMA.

Figure 1 shows the structures of two representative polymer ligands along with the nucleophile precursors used. Synthesis of LA/His-PIMA-ZW was carried out by reacting PIMA with a

https://dx.doi.org/10.1021/acs.bioconjchem.0c00169
Bioconjugate Chem. 2020, 31, 1497−1509

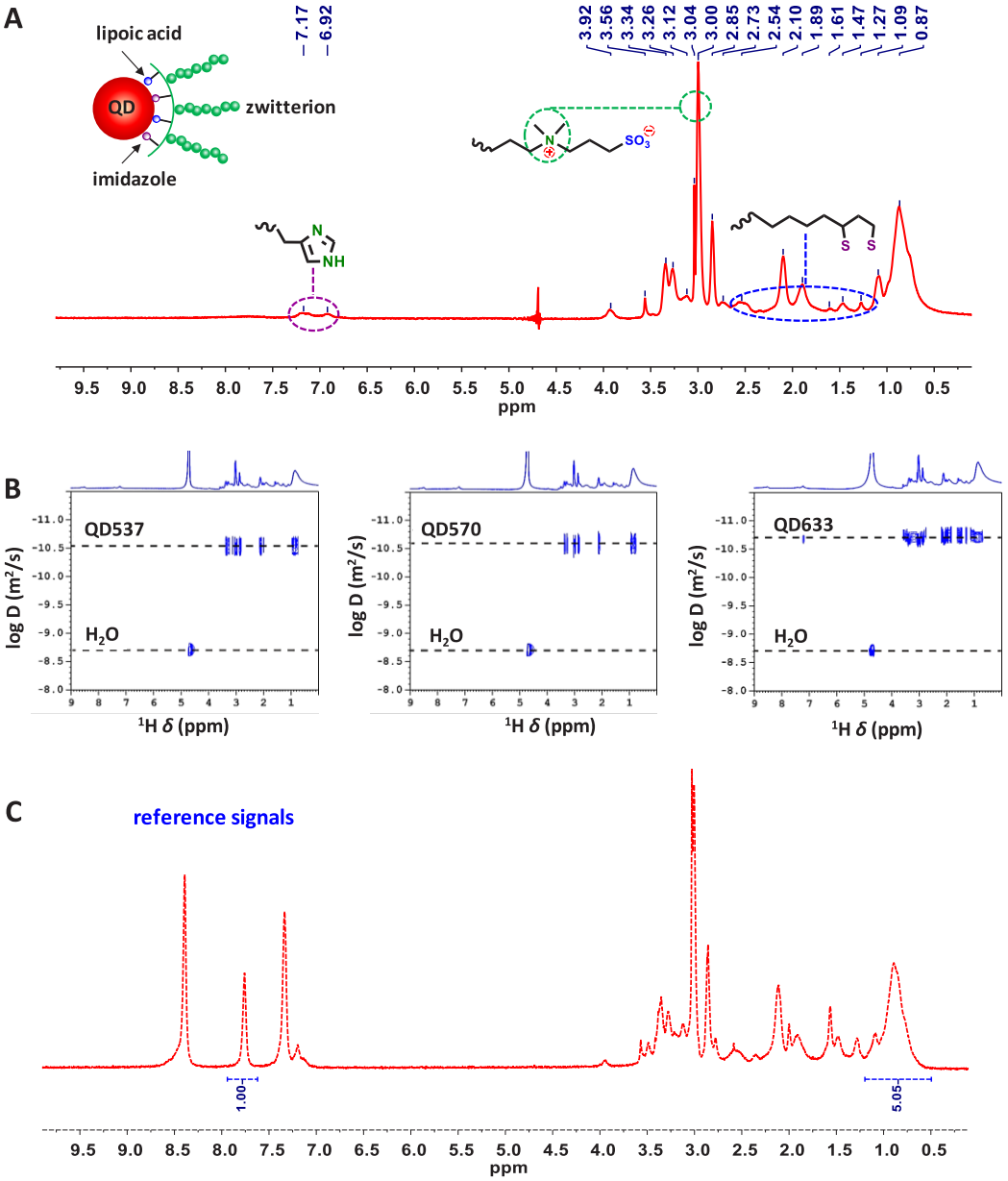

Figure 3. (A) Pulsed-field gradient-based water suppression ^{1}H NMR spectrum collected from LA/His-PIMA-ZW-coated QDs in D_2O. Assignment of the protons associated with each functionality are labeled on the spectrum. (B) 2D DOSY contour plots collected from LA/His-PIMA-ZW-coated QD537, LA/His-PIMA-ZW-coated QD570, and LA/His-PIMA-ZW-coated QD633 in D_2O. (C) Ligand counting: pulsed-field gradient-based water suppression ^{1}H NMR spectrum of LA/His-PIMA-ZW-capped QD537, calibrated with respect to pyridine serving as a standard.

stoichiometric mixture of lipoic acid-amine (20%), histamine (30%), and zwitterion-amine (50%). This introduces ~8 lipoic acid groups, ~12 imidazole anchors, and ~20 zwitterion moieties, while releasing ~40 carboxylic acids along the polymer backbone.[45] Synthesis of LA/His-PIMA-ZW/N_3 was carried out by substituting a fraction of the zwitterion-amine (15%) with H_2N-TEG-N_3 during the reaction, yielding a ligand coating readily compatible with "click" chemistry.

This design has indeed yielded polymer ligands that can be applied for coating QDs using a UV-promoted ligand exchange strategy (i.e., photoligation), which is effective and simple to implement. This strategy exploits the photochemical sensitivity of the strained dithiolane rings to UV irradiation that overlaps with the lipoic acid absorption band centered at ~340 nm, as this breaks the disulfide bond and rapidly promotes ligand coordination onto the QDs *in situ*.[55,56] We applied this photoligation strategy to the QDs using the new ligands (Figure 1C). First, mixing the hydrophobic QDs and ligands in organic phase for 2 h promotes imidazole-driven coordination of the polymer onto the QD surfaces and displacement of the native cap, allowing for a phase transfer of QDs to water. Second, applying UV irradiation to aqueous QD dispersions for 30 min readily triggers ligation of the photomodified anchors onto the nanocrystals, yielding mixed coordination coating. This method is simpler than the approach developed in our previous report for photoligation of QDs with LA-PIMA-ZW ligands.[52]

Characterization of Hydrophilic QDs. The purified polymer-coated QDs were characterized using a combination of UV−visible absorption, fluorescence spectroscopy, FT-IR,

https://dx.doi.org/10.1021/acs.bioconjchem.0c00169
Bioconjugate Chem. 2020, 31, 1497−1509

along with 1D ^{1}H NMR and 2D diffusion-ordered spectroscopy (DOSY). In particular, the NMR experiments were exploited to confirm the effectiveness of photoligation to fully substitute the native ligands with the polymers, to extract a measure for the diffusion coefficient and hydrodynamic radius of the hydrophilic nanocrystals, and to extract an estimate of the number of ligands in a QD coating.

Optical Characterization. Figure 2A shows the absorption and emission spectra collected from three representative dispersions of QDs emitting at 537, 570, and 633 nm, before and after photoligation with LA/His-PIMA-ZW. The spectra of the hydrophilic QDs in water are essentially identical to those collected from their hydrophobic counterparts dispersed in hexane, indicating that the structural and optical integrity of the nanoparticles were preserved following phase transfer. Similar data were collected from QDs photoligated with LA/His-PIMA-ZW/N_3. The beneficial effects of the mixed coordination polymers on the QD properties were further evaluated by comparing the PL intensities measured for the hydrophobic and hydrophilic QD dispersions with similar optical densities. The PL intensities measured for aqueous dispersions were ∼85%−95% of that recorded for hydrophobic ones in hexane, indicating that marginal PL losses are measured after phase transfer. This result can be attributed to the benefits of introducing imidazole anchors, which provide better passivation of the surface defect states and reduce the effects of nonradiative decay channels.[45,57]

FT-IR Characterization. Efficiency of the ligand exchange along with integrity of the azide groups on the QD surfaces were verified by FT-IR spectroscopy. Figure 2B shows a side-by-side comparison between the FT-IR spectra collected from pure polymers (LA/His-PIMA-ZW and LA/His-PIMA-ZW/N_3) and from QDs photoligated with either of those ligands. In each case, the spectrum of the QD sample exhibited nearly identical patterns to that of the pure ligands. In particular, a clearly defined band at ∼2100 cm^{-1} was measured for the LA/His-PIMA-ZW/N_3 and the polymer-coated QD samples, attributed to the asymmetric vibration of the azide groups in the coating. These results confirm the success of the ligand exchange and the availability of intact azide groups on the QD surfaces for further conjugation.

1D ^{1}H NMR and 2D Diffusion-Ordered Spectroscopy. The NMR data not only were used to provide further proof for a complete ligand exchange and to extract estimates for the diffusion coefficient of hydrophilic QDs but also to quantify the number of ligands per nanocrystal. Figure 3A shows the ^{1}H NMR spectrum collected from a representative QD dispersion in D_2O. The spectrum shows distinct peaks over the range 1.1−2.5 ppm attributed to the lipoic acid protons, two resonances at ∼6.9 and ∼7.2 ppm ascribed to the protons on the imidazole rings, and a pronounced resonance at 3.0 ppm corresponding to the methyl groups of the zwitterion moieties. In addition, a broad peak at ∼0.9 ppm ascribed to the methyl groups on the PIMA backbone was measured. The proton peaks shown in Figure 3A for the polymer-QDs are broadened and slightly weakened compared to those shown in the spectra of LA-NH_2 and ZW-NH_2 provided in the Supporting Information (Figure S1). Such broadening is expected for the QD samples, due to the combination of the polymeric nature of LA/His-PIMA-ZW and the slower dynamics of protons in the QD-bound ligands.[58,59] We also note that no signatures associated with the native capping molecules (e.g., trioctyl phosphine (TOP), trioctyl phosphine oxide (TOPO), n-hexylphosphonic acid (HPA), and 1-hexadecyl amine (HDA)) were measured in the QD samples, which clearly proves that the hydrophobic ligands were displaced by the polymer coating during ligand exchange.[45,58]

Further confirmation that the ^{1}H NMR signatures measured from the QD samples originate from bound ligands and not from excess free ligands in the medium, was deduced from DOSY experiments. DOSY can exploit the dependence of the specific NMR features of active atoms in molecules of interest on the magnetic field gradient, providing a measure of the translational diffusion of those molecules in solution.[60] The diffusion-weighted ^{1}H NMR spectra can be collected by selectively filtering out the fast diffusing species with a magnetic field gradient.[61,62] Attenuation of the signal (often referred to as the echo intensity), I_G, can be described in its simplified form using the Stejskal−Tanner equation:[63−65]

$$I_G = I_0 \exp\left(-\gamma^2 G^2 \delta^2 \left(\Delta - \frac{\delta}{3}\right) D\right) \quad (1)$$

where D is the diffusion coefficient ascribed to the peak proton(s), γ is the proton gyromagnetic ratio, G is the strength of the magnetic gradient pulse, δ is its duration, Δ is the time interval between two bipolar gradient pulses, and I_0 is the signal at zero gradient. Using this technique, the Brownian diffusion coefficient(s) associated with the proton features can be measured. This also provides a means of distinguishing freely diffusing ligands from those QD-bound, based on difference in the measured diffusion coefficients; free ligands would exhibit faster diffusion coefficient than surface bound ones. Thus, by tracking changes in the intensity profile with the applied gradient field strength collected from dispersions of QD-bound ligands only, one can extract a measure of D for the nanocrystals in the sample. Figure 3B shows representative DOSY contour spectra collected from purified dispersions of QD537, QD570, and QD633 ligated with LA/His-PIMA-ZW in D_2O. Data show that the various proton signals in each spectrum can be associated with two distinct diffusion coefficients. The slower ones are attributed to the surface-bound polymers for each set of QDs; these values are much smaller than that measured for water molecules in the sample. More precisely, the data compiled in Table 1 show that the diffusion coefficient decreases systematically from ∼3.36 × 10^{-11} m^2 s^{-1} for QD537 and ∼3.03 × 10^{-11} m^2 s^{-1} for QD570 to ∼2.72 × 10^{-11} m^2 s^{-1} for QD633, while a value of ∼2.0 × 10^{-9} m^2 s^{-1} was extracted for water molecules. In each spectrum, only one diffusion coefficient associated with the polymer proton resonances was measured, which is about 2−3

Table 1. Values of Diffusion Coefficient, Hydrodynamic Radius, and Number of Ligands Per QD Measured for Each Size of QDs Ligated with LA/His-PIMA-ZW, Extracted from the NMR Analyses

QD	radius [nm][a]	molar extinction coefficient [M^{-1} cm^{-1}][b]	diffusion coefficient [m^2 s^{-1}]	R_H [nm]	ligands/QD
QD537	∼3.0	6.06 × 10^5	3.36 × 10^{-11}	6.4	∼15
QD570	∼3.4	1.07 × 10^6	3.03 × 10^{-11}	7.1	∼21
QD633	∼4.0	2.47 × 10^6	2.72 × 10^{-11}	7.9	∼32

[a]The values of the QD radii were extracted from small-angle X-ray scattering data based on previous report.[68] [b]The molar extinction coefficients were determined using the absorbance at 350 nm.[68−70]

https://dx.doi.org/10.1021/acs.bioconjchem.0c00169
Bioconjugate Chem. 2020, 31, 1497−1509

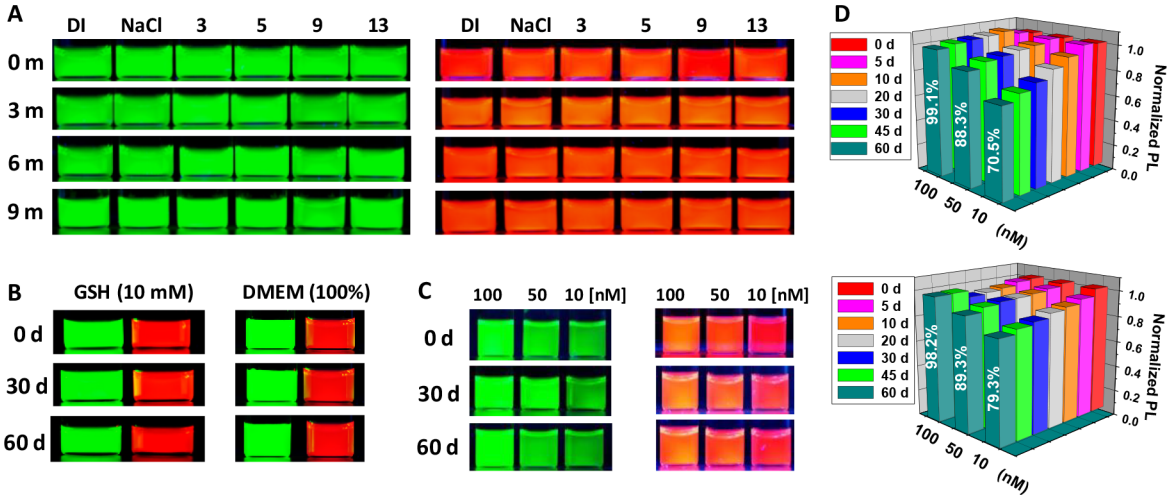

Figure 4. Colloidal stability tests: (A) QD537 and QD633 ligated with LA/His-PIMA-ZW dispersed in DI water, NaCl solution (1 M), and phosphate buffer (20 mM) at pH from 3 to 13 over nine months of storage. (B) LA/His-PIMA-ZW-coated QD537 and QD633 in dispersion containing 10 mM glutathione (GSH) and mixed with 100% growth media (DMEM) stored at ∼4 °C and tracked for two months. (C and D) QD dispersions at different concentrations (100, 50, and 10 nM) stored under ambient conditions, along with the time progression of the PL intensities tracked over two months.

Table 2. Comparison between Several Polymer Coatings: Ligand Structures Correlated to the QD Hydrodynamic Radius, Fluorescence Property, and Colloidal Stability

QD	ligand	anchor	hydrophilic unit	R_H [nm]	relative PL [%][a]	PL [10 nM, 60 d][b]	pH < 5	against photo-oxidation
QD537	His-PIMA-PEG[45]	imidazole	PEG	10.3	76	NA	no	yes
QD537	LA-PIMA-PEG[45]	lipoic acid	PEG	11.3	75	NA	yes	no
QD537	LA/His-PIMA-PEG[45]	mixed	PEG	10.9	96	NA	yes	yes
QD537	His-PIMA-ZW[33]	imidazole	ZW	5.2	89	49%	no	yes
QD537	LA-PIMA-ZW[52]	lipoic acid	ZW	6.6	70	37%	yes	no
QD537	LA/His-PIMA-ZW	mixed	ZW	6.4	91	70%	yes	yes

[a]The influence of different polymer coatings on the QD fluorescence was assessed by comparing the PL intensity of polymer-coated QDs to the hydrophobic QDs in hexane at the same optical density. [b]Colloidal stability of QDs at low concentration (10 nM) were evaluated by comparing their PL intensities after 60 days of storage to the fresh samples. The chemical structures of the polymer ligands, His-PIMA-PEG, LA-PIMA-PEG, LA/His-PIMA-PEG, His-PIMA-ZW, and LA-PIMA-ZW, are provided in the Supporting Information.

times slower and approximately 2 orders of magnitude smaller than those of freely diffusing organic ligands and water molecules, respectively.[65] This clearly indicates that there are no detectable free ligands in the dispersions.[58,59] This further confirms the strong coordination of the ligand and the effectiveness of phase transfer protocols used.

Combining data of the diffusion coefficients with the Stokes−Einstein equation,

$$D = k_B T/(6\pi\eta R_H) \quad (2)$$

where k_B is the Boltzmann constant, T is the absolute temperature, and η is the dynamic viscosity of the medium,[66,67] yields a measure for the hydrodynamic radius of the nanoparticles (R_H). The extracted hydrodynamic radius is ∼6.4 nm for QD537, ∼7.1 nm for QD570, and ∼7.9 nm for QD633, respectively. These values agree with our previous reports for zwitterionic coatings but are smaller than PEGylated coatings (∼10−11 nm for QD537).[33,45]

We also exploited the ^{1}H NMR data collected from the QDs to extract the number of ligands per QD, by comparing the total concentration of ligands to that of the QDs in the sample. This information is critical, as ligand density not only greatly influences the colloidal stability of the nanoparticles but also strongly impacts their performance in biological investigations.[71,72] The ligand concentration was extracted from a comparison of the integration of the methyl proton peak at ∼0.9 ppm in the polymer with the integration of γ-proton peak at ∼7.7 ppm emanating from pyridine standard (Figure 3C). Conversely, the QD concentration was calculated from the absorbance at 350 nm combined with the molar extinction coefficients of the core−shell QDs.[68−70] Such analysis indicates that there are ∼15 ligands per QD537, ∼21 ligands per QD570, and ∼32 ligands per QD633 (Table 1). This trend is consistent with the increase in the surface area per nanocrystal for larger sized QDs, requiring more ligands for stabilization. These values are also consistent with previous results from our group, where green-emitting QDs stabilized with PEGylated polymer ligands (i.e., PEG_{750} motifs) were characterized.[33] Finally, using the above NMR data and assuming that 15% of the functional groups are made from NH_2-TEG-N_3, we estimate that the number of "clickable" azide groups on a QD633 photoligated with LA/His-PIMA-ZW/N_3 is ∼190. Additional ^{1}H NMR spectra used for ligand counting are provided in the Supporting Information (Figure S2).

Colloidal Stability Tests. The colloidal stability of two representative sets of QDs photoligated with LA/His-PIMA-ZW was evaluated under a few biologically relevant conditions, including the pH range 3−13, a high concentration of electrolyte (1 M NaCl), in the presence of cell culture media (100% Dulbecco's modified Eagle medium, DMEM), in 10

https://dx.doi.org/10.1021/acs.bioconjchem.0c00169
Bioconjugate Chem. 2020, 31, 1497−1509

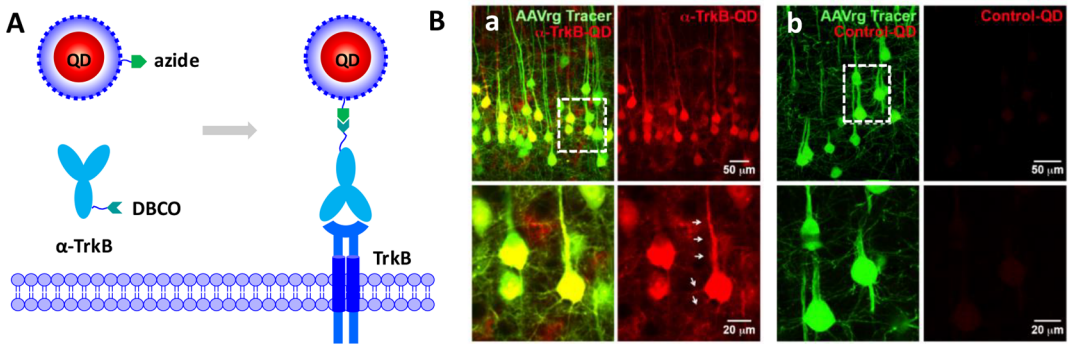

Figure 5. (A) Schematics of the click-promoted conjugation of QDs to anti-TrkB antibody. (B) QD-immunolabeling of TrkB in corticospinal neurons within the M1 motor cortex visualized by AAVrg (green): (a) strong labeling by α-TrkB-QDs (red), where fine apical and basilar spine morphology of individual neurons are apparent (arrows); (b) no labeling was observed when using control QDs.

mM glutathione, and when stored at nanomolar concentrations (10, 50, and 100 nM) under ambient conditions (room temperature and light exposure).

Figure 4A shows the fluorescence images collected from QD537 and QD633 (0.3 μM) dispersed in buffers at pH 3−13, in 1 M NaCl solution, and tracked with time storage at ∼4 °C. All dispersions stayed homogeneous and highly fluorescent, with no sign of microscopic aggregation or visual fluorescence loss for at least nine months. The stability of QDs was also assessed in the presence of 10 mM glutathione and in 100% cell growth media, where no aggregation could be detected after at least two months of storage (Figure 4B). We further tested the colloidal stability of the QD dispersions at very low concentrations including 10, 50, and 100 nM under ambient conditions. The fluorescence images shown in Figure 4C indicate that both sets of QDs stayed fluorescent and aggregate-free at all tested concentrations. The time progression of PL intensities in Figure 4D show that the fluorescence of the 100 nM dispersions was essentially unchanged with storage time for both sets. At lower concentrations (50 and 10 nM), the PL intensities were slightly decreased but dispersions remained highly fluorescent for at least two months. For example, the relative PL was ∼88% for green QDs and ∼89% for red QDs compared to the emission from fresh samples at 50 nM, whereas dispersions of QD537 and QD633 at 10 nM preserved about 70% and 80% of their emission during the same period.

Table 2 provides a contextual comparison showing the effects of ligand structure on the colloidal and photophysical stability for the present polymer ligand and those reported in our previous works (shown in Figure S3).[33,45,52] Compared with polymer ligands presenting only one type of anchors (e.g., LA-PIMA-ZW or His-PIMA-ZW), the mixed coordination ligands generate QDs with higher fluorescence, better colloidal/photo stability in acidic pHs, and low concentrations, under ambient conditions over extended storage time. Furthermore, given the molecular nature of the zwitterion motif, LA/His-PIMA-ZW-coated QDs are inherently compact compared with those coated with PEGylated polymers (e.g., LA/His-PIMA-PEG). These comparisons provide additional evidence that the LA/His-PIMA-ZW ligands yield highly compact QDs with better colloidal stability over several conditions, a result attributed to the enhanced coordination of imidazole and lipoic acid anchors and the strong affinity of the zwitterion motifs to water.

Immunolabeling and Live Cell Imaging. Strain-promoted cycloaddition (Click) chemistry provides exquisite chemoselectivity, high efficiency, and fast reaction rates, even under complex conditions.[73,74] It has progressively become one of most effective approaches for nanoparticle bioconjugation.[52,75,76] Here, we apply this strategy to conjugate LA/His-PIMA-ZW/N_3-coated QDs (emitting at 633 nm) with dibenzocyclooctyne (DBCO)-labeled proteins and to test their effectiveness in immunofluorescence staining and live cell imaging. The average number of antibodies per QD (or the valence of the QD-conjugate) has been estimated using Pierce BCA protein assay; α-TrkB-QD conjugates were used for the analysis. A valence of ∼1.12 was deduced (see the Supporting Information, Table S1 and Figure S4). We should note that the reported value is an average valence, but the conjugates are individually heterogeneous and well described by Poisson distribution.[77]

Immunolabeling of BDNF-Receptor TrkB in Cortical Tissue. Tropomyosin receptor kinase B is the high affinity receptor for BDNF mediating neuronal differentiation and survival. BDNF initiates signaling by binding to TrkB, where this complex is internalized and retrogradely transported to the cell soma.[78] Combining strain-promoted click chemistry with the high affinity coating, we demonstrated the conjugation of red-emitting QDs to anti-TrkB antibody, yielding fluorescent probes for efficient labeling of TrkB in corticospinal neurons within cortical tissue. As shown in Figure 5B, left panel, α-TrkB-QD conjugates (3 nM) specifically labeled the pyramidal neurons in layer V of the cortical tissue slice, where the red QD fluorescence was fully colocalized with the fluorescence of AAVrg (green color), a marker used for visualization of the neurons. In contrast, control QDs coated with LA/His-PIMA-ZW/N_3, without conjugation to antibodies, yielded no labeling of the pyramidal cells (Figure 5B, right panel). Additionally, specific labeling for TrkB can be observed within the apical dendritic spines as well as basilar spines of layer V (arrows, Figure 5B). The efficient labeling of TrkB in corticospinal neurons within the M1 motor cortex indicates that such QD probes can be readily applied for immunolabeling proteins of interest.

Live Cell Imaging of Internalized BDNF-QDs. The complex nature of BDNF existing in pre, pro, and mature states has allowed this small neurotrophin to play diverse roles in neurogenesis, synaptic plasticity, long-term potentiation, and neuron survival, to name a few.[79−82] However, the heterogeneity of this protein also leads to contradictive

https://dx.doi.org/10.1021/acs.bioconjchem.0c00169
Bioconjugate Chem. 2020, 31, 1497−1509

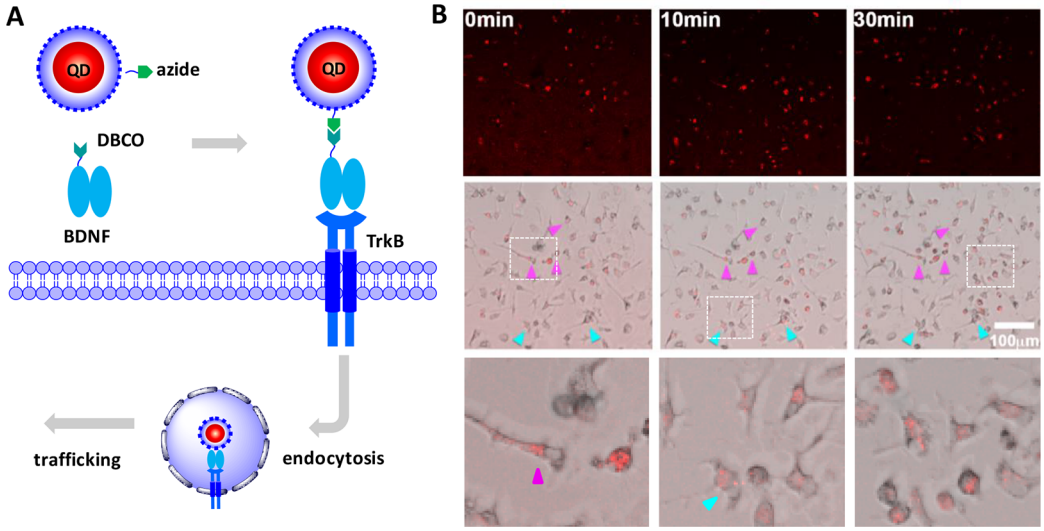

Figure 6. (A) Scheme of click conjugation of QDs to BDNF. (B) Live neuron cell imaging of BDNF-induced TrkB endocytosis and activation of signaling over time. QD fluorescence images (top panel), composite images of QD fluorescence and differential interference contrast (middle panel), and enlarged composite images (bottom panel) are shown.

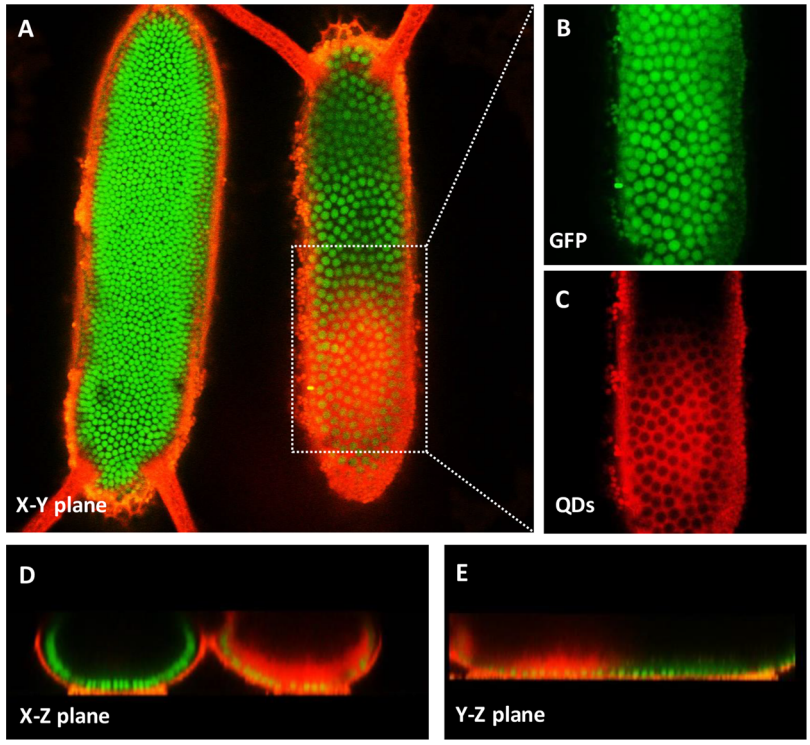

Figure 7. (A) Overlaid fluorescence images (lower focal plane) of two *Drosophila melanogaster* embryos recorded upon injection of QDs into the right one. (B and C) GFP fluorescence distribution in embryo nuclei and QD fluorescence distribution in plasma membranes in high magnification images. (D and E) Reconstructions of the spatial fluorescence distribution on two vertical planes ($X-Z$ plane and $Y-Z$ plane).

findings with irreproducible results that have cast a shadow on advancing our understanding of the properties of pro-BDNF and mature-BDNF. The mature-BDNF binds preferentially to the TrkB receptor, activating signaling cascades responsible for neuronal survival and synaptic plasticity. Here, we show that a QD conjugated to the mature-BDNF *via* click chemistry provides a fluorescent probe that is capable of monitoring the BDNF-induced TrkB endocytosis and activation of signaling pathways downstream of TrkB in live adult neuronal cells. Figure 6 shows representative time-lapse fluorescence images for BDNF internalization; the full set of images acquired at 5 min intervals is provided in the Supporting Information, Figure S5. The images show that the mature-BDNF-QDs (3 nM) were rapidly uptaken in live cultures of cortical neurons. A few neurons displayed an almost instant uptake of the neurotrophin (pink arrows), where all cells that internalized BDNF-QDs did so within 10 min (blue arrows). Moreover, BDNF-QDs could be seen localizing within axons at 10−30 min and dispersing throughout the cell at 30 min. In contrast, little to no uptake of QDs was observed for the control without BDNF

https://dx.doi.org/10.1021/acs.bioconjchem.0c00169
Bioconjugate Chem. 2020, 31, 1497−1509

conjugation (see the Supporting Information, Figure S6). Benefitting from the compact size of QDs coated by zwitterionic ligands, this chemistry can be further applied by comparing the pre, pro, or mature forms of BDNF in various disease states for future study.

***In Vivo* Embryo Imaging.** The use of QD probes for *in vivo* imaging and tracking continues to generate much interest, but questions pertaining to the nanocrystal colloidal and photophysical stability in those conditions and their effects on the viability of cells and organisms are still not understood. We examined the *in vivo* stability and cytotoxicity of LA/His-PIMA-ZW-coated QDs delivered to *Drosophila melanogaster* embryos *via* microinjection.

The embryo encoded with GFP in the nuclei of all cells was microinjected with 2.6 μM red-emitting QDs diluted in Dulbecco's PBS buffer, 120 min after the egg laying (stage 3−4). The representative fluorescence images of two embryos, collected at lower and upper focal planes, are shown in Figure 7A and Figure S7 (Supporting Information), respectively. The embryo injected with QDs shows a strong red fluorescence signal overlaid with the green signal from the GFP-labeled nuclei. The formation of the cellular blastoderm can be visualized under high magnification (Figure 7B,C). The uniform circular shapes in the red fluorescence patterns suggest that QDs associated with the plasma membranes that assembled during cell cycle 14 around the many nuclei to form individual cells.[83] The reconstructed fluorescence images collected by scanning the focal plane in the dorsoventral direction (X−Z plane) and posteroanterior direction (Y−Z plane) indicate that the QDs localized predominantly in the cellular blastoderm developed at the periphery of the embryo (Figure 7D,E). The sequential images acquired up to 150 min after injection reveal that the QDs remained strongly fluorescent and homogeneously distributed in the embryo (Supporting Information, Figure S8). The cells in the embryo appeared to be unperturbed and continued the embryogenesis during the experimental cycle, indicating that the polymer-coated QDs elicited minimal to no toxicity. The observed colloidal stability of the polymer-coated QDs inside the embryos should be contrasted with what was measured for QDs coated with monomeric DHLA, the smallest version of LA-based ligands devoid of a hydrophilic motif.[84] Punctate fluorescence staining rapidly developed inside cells micro-injected with these materials, suggesting nanoparticle aggregation.

Clearly, the present ligand coating combining zwitterion motifs and mixed coordination offers great benefits for integrating luminescent QDs and potentially other nanocolloids in biological imaging. In addition to the effectiveness of the synthetic route used, the present ligands impart onto the nanocrystal high colloidal stability, enhanced PL properties across a wide range of conditions, and ease of conjugation to biomolecules. They are optimally suited for implementing chemical coupling relying on the selective and efficient click chemistry, to prepare stable and highly fluorescent α-TrkB-QD and BDNF-QD bioconjugates. Indeed, we found that α-TrkB-QD conjugates allowed for the immunostaining of the pyramidal neurons in cortical tissue with high efficiency, while BDNF-QD conjugates permitted tracking of the time-dependent receptor-induced endocytosis by live neurons. We also found that the newly prepared zwitterion-coated QDs stay homogeneously distributed in live embryos while eliciting no measurable cytotoxicity. These results are promising, and the prepared materials can find use in other imaging and tracking experiments where a rather small size, high fluorescence, and compatibility with chemoselective conjugation strategy could advance our understanding of important problems in neuroscience and biomedicine.

CONCLUSION

We have prepared a set of multifunctional polymers that combine mixed coordination with a zwitterion hydrophilic motif and applied them for the coating and conjugation of luminescent QDs to an antibody and ligand targeting specific neuron cell receptors. Combining this ligand design with photochemical ligation yielded hydrophilic QDs that exhibit high fluorescence and excellent colloidal stability over a broad range of conditions and are readily applicable for conjugation to biomolecules. The polymer coating has been characterized using 1D ^{1}H NMR and 2D DOSY spectroscopy to extract estimates for the hydrodynamic radius and surface ligand density. Introduction of azide groups into the ligand has facilitated the assembly of QD-bioconjugates using the selective click reaction. The formed α-TrkB-QD conjugates provided efficient immunolabeling of TrkB receptors in pyramidal neurons within cortical tissue, while the BDNF-QD conjugates were used for imaging the activation of BDNF/TrkB signaling in live adult neuron cultures. We also investigated the effects of microinjecting the QDs in *Drosophila melanogaster* embryos and found that *in vivo* the polymer-coated QDs were colloidally stable, exhibited no measurable toxic effects, and allowed for visualization of cellular distribution in such embryos. We should emphasize that the present chemical route can be easily applied to prepare ligands that are optimally adapted for coating a variety of other nanocolloids, such as those made of gold, silver, and magnetic cores. The present coating strategy combined with the ease and selectivity of the click-based conjugation offer great potential for the integration of various nanocolloids in an array of biological applications.

EXPERIMENTAL SECTION

Synthesis of Polymer Ligands. *Synthesis of LA/His-PIMA-ZW.* In a 50 mL round-bottom flask, PIMA (0.385 g, 2.5 mmol of monomer units) was dissolved in 5 mL of dimethyl sulfoxide (DMSO). The solution was purged with nitrogen and heated to 45 °C using an oil bath. Histamine (0.083 g, 0.75 mmol) dissolved in 1 mL of DMSO was added to the PIMA solution *via* a syringe, followed by adding 1 mL of DMSO solution containing LA-NH_2 (0.124 g, 0.5 mmol). After that, 1 mL of DMSO containing ZW-NH_2 (0.281 g, 1.25 mmol) was added. The reaction mixture was left stirring at 45 °C overnight under nitrogen flow. The solution was concentrated to ∼2 mL under vacuum, and 20 mL of acetone was added to precipitate the compound. After centrifugation for 5 min at 3700 rpm, the solvent was decanted and the solid pellet was washed twice with acetone and dried under vacuum. This provided the final product as white-yellowish solid with a final yield of ∼90%.

Synthesis of LA/His-PIMA-ZW/N_3. This compound was synthesized following the same steps described above, except that 15% ZW-NH_2 was substituted with H_2N-TEG-N_3; the final yield was ∼83%.

Ligand Exchange. In a 10 mL scintillation vial, hydrophobic QDs (∼2 nmol) were precipitated with 3 mL of

https://dx.doi.org/10.1021/acs.bioconjchem.0c00169
Bioconjugate Chem. 2020, 31, 1497−1509

ethanol and then centrifuged at 3600 rpm for 6 min. The QD pellet was redispersed in 250 μL of chloroform. Separately, 20 mg of the polymer ligands were dissolved in 180 μL of DMSO. A gentle heating and sonication can accelerate ligand dissolution. The solution was added to the QD dispersion, and the mixture was stirred at room temperature for 2 h (or at 4 °C overnight for convenience). Chloroform (300 μL) and 300 μL of methanol were added to the QD dispersion, followed by 3.5−4 mL of hexane. The mixture was sonicated for ∼20 s and centrifuged at 3600 rpm for 7 min. The supernatant was removed using a pipet, and the above purification steps were repeated one more time. The QD pellet was dried under a vacuum for 10−15 min and mixed with 2 mL of DI water, followed by the addition of 25 μL of aqueous NaOH solution (2.5 M). After sonication, a clear QD dispersion was obtained. The vial was sealed with a rubber septum, and the atmosphere was switched to nitrogen by applying 2−3 rounds of a mild vacuum followed by flushing with nitrogen. The vial was then placed inside the UV photoreactor and irradiated for 30 min while stirring. This promoted a photoinduced reduction of the lipoic acid groups in the ligand.[55] The QD dispersion was passed through a syringe filter (∼0.45 μm) and then to a centrifugal filtration device (Millipore, cutoff = 50 kDa, volume = 15 mL). Excess free ligands were removed by applying 3−4 rounds of concentration/dilution with DI water. Ligand exchange with LA/His-PIMA-ZW/N_3 was carried out following the same steps, except that 25 mg of polymer ligands was used.

NMR Characterization. ^{1}H NMR spectra were collected using pulsed-field gradient water suppression experiments. After phase transfer and during the purification step of the QDs, DI water was switched to D_2O by applying two rounds of concentration/dilution using deuterium oxide (2 mL each). The final volume of the QD dispersions was adjusted to 500 μL. The QD concentration used for collecting ^{1}H NMR spectra was ∼8−9 μM, as determined by UV−vis absorption data; the reported NMR spectra were the average over 500 scans. The above samples were also used to acquire the diffusion-ordered spectroscopy data. In our experiments, the absolute temperature and the dynamic viscosity of the medium were 293 K and ∼1.002 × 10^{-3} N s/m^2 (∼1 cP), respectively. NMR characterization of the ligand density was carried out using dispersions in D_2O, supplemented with 2 μL of pyridine (24.8 μmol) dissolved in 5 μL of D_2O, to provide a standard. We should note that the final QD concentrations in the NMR samples were slightly reduced with the addition of pyridine, a fact that was taken into accounted during analysis.

Click Conjugation of QDs with α-TrkB and BDNF. The various QD conjugates were prepared by reacting LA/His-PIMA-ZW/N_3-coated QDs with α-TrkB or BDNF proteins labeled with dibenzocyclooctyne. QDs emitting at 633 nm were used for these experiments.

Preparation of α-TrkB-QD Conjugates. α-TrkB (20 μg, 0.143 nmol) was first reacted with DBCO-sulfo-NHS ester (1.88 mM, 0.38 μL) in 100 μL of HEPES buffer (pH 7.4, 25 mM) for 30 min at room temperature; this represents a 5-fold molar excess of DBCO with respect to the antibody. An aliquot of QD dispersion (12 μM, 8 μL) was then added to the antibody solution, corresponding a QD/α-TrkB molar ratio of 1:1.5. The mixture was stirred at 4 °C overnight, and the conjugates were purified using a PD-10 column.

Preparation of BDNF-QD Conjugates. First, lyophilized BDNF powder (15 μg, 0.55 nmol) was dissolved in 100 μL of HEPES buffer (pH 7.4, 25 mM) and reacted with 5-fold molar excess of DBCO-sulfo-NHS ester (1.88 mM, 1.47 μL) at room temperature for 30 min. Next, an aliquot of QD dispersion (12 μM, 23 μL) was added to the protein solution; the molar ratio of QD/BDNF was 1:2. The mixture was left stirring at 4 °C overnight. The BDNF-QD conjugates were purified from unreacted protein and byproducts using a PD-10 column. The purified QD conjugates were characterized by gel electrophoresis and ζ-potential analysis (see the Supporting Information).

Tissue Preparation and Immunofluorescence Imaging. The US National Institutes of Health guidelines for laboratory animal care and safety were strictly followed. All surgeries of mice were done under deep anesthesia using isoflurane gas followed by postoperative care. Corticospinal neurons were visualized in the motor cortex by retrogradely tracing at C8 spinal cord level with AAVrg virus (7×10^{12} genome copies/mL, Addgene 59462) at 0.8 mm depth, 0.5 mm lateral from midline, with a micropipette where injection pressure and duration were controlled by PicoSpritzer II (General Valve, Fairfield, NJ). Mice were perfused 7 days later with 4% PFA and tissue removed and cryoprotected in 30% sucrose in PBS. Cortical tissue was sectioned on a microtome at 35 μm intervals and permeabilized in 0.25% triton in 5% donkey serum for 1 h rotating at room temperature. The tissue was incubated in pre-blocked α-TrkB-QD conjugates (3 nM) or QD-control (3 nM) diluted in 5% donkey serum overnight at 4 °C. Next day, the tissue was rinsed in 1X PBS three times, with a 10 min wash each, and mounted onto microscope slides. Images were collected on a Zeiss LSM 880 confocal microscope with 20× objective (Zeiss). Z-stack images were taken across 13−15 μm of tissue at optimal intervals, with 1024 × 1024 resolution, averaging 4 lines per section, sequentially scanning at 405 nm with a detector range at 611−689 nm for QDs. Max projection images were used in the shown Figures.

Live Neuronal Cell Imaging. Cerebral cortices were isolated from C57BL/6 mice at postnatal day 30 and transferred to cold D-PBS, where intact cortices were placed into C-tubes (Miltenyi, 130-096-334, Bergisch Gladbach, Germany) with appropriate buffers and dissociated according to brain dissociation protocol (Miltenyi, 130-107-677) using the gentleMACS Octo dissociator with heaters. Cells were plated onto Nunc LabTEKII chamber slides coated with poly-D-lysine (10 μg/mL) and laminin (10 μg/mL) and were cultured for 7 days *in vitro* in MACS neuro media supplemented with B27 (Life tech 12587010, Carlsbad, CA), 10% FBS (Genesee Sci 25-514H, San Diego, CA), and 0.02 μg/mL BDNF (Peprotech 450-02, Rocky Hill, New Jersey). Images were captured with a 20× objective, Leica Sp8 lightning confocal microscope (Leica Microsystems). Images were acquired at 5 or 10 min intervals after the BDNF-QDs were introduced into the live cultures at 3 nM. Phase contrast images were taken simultaneously, with excitation at 405 nm set to 2% power and emission spectrum set to 600−700 nm. An average of four lines were taken per image, at 1024 × 1024 resolution.

***In Vivo* Imaging of *Drosophila melanogaster* Embryos.** *Drosophila melanogaster* embryos expressing nuclei-targeted green fluorescent protein (GFP) in all cells (Stock #1691, Bloomington Drosophila Stock Center NIH P40OD018537) were prepared for the imaging experiments following the literature protocol.[85] Specifically, fertilized egg

https://dx.doi.org/10.1021/acs.bioconjchem.0c00169
Bioconjugate Chem. 2020, 31, 1497−1509

cells were collected after 60−120 min from laying (stage 2−4), deposited on glass slides, and maintained in a desiccator together with $CaSO_4$ at ambient temperature for 8 min. The slides were then covered with a mixture of Series 700 (Sigma H8898) and Series 27 (Sigma H8773) halocarbon oils (7:1, v/v) and were transferred individually onto the stage of a Leica DMIL LED inverted microscope. The solution of QDs (2.6 μM) diluted in Dulbecco's PBS (pH = 7.4) were injected into the embryos at stage 3−4, with a MN151 Narishige micromanipulator. The slides were mounted on the stage of a Leica SP5 confocal laser-scanning microscope and imaged. The fluorescence of GFP was detected with an excitation wavelength of 488 nm and an emission wavelength of 500−550 nm. The fluorescence of QDs were detected with an excitation wavelength of 561 nm and an emission wavelength of 575−650 nm. $X-Z$ and $Y-Z$ plane fluorescence images were recorded by scanning the focal plane in the dorsoventral direction (scan step = 3 μm), together with reconstructions of the spatial fluorescence distribution on two vertical planes.

■ ASSOCIATED CONTENT

Supporting Information

The Supporting Information is available free of charge at https://pubs.acs.org/doi/10.1021/acs.bioconjchem.0c00169.

Discussions of materials and instrumentation used, growth of QDs, synthesis steps, and BCA protein assay, table of raw data and absorbance values, and figures of NMR spectra, chemical structures, agarose gel electrophoresis image, ζ-potential values, white light image, standard curve assembled from the BCA assay, absorption data summary, time-lapse fluorescence images, and overlaid fluorescence images (PDF)

■ AUTHOR INFORMATION

Corresponding Author

Hedi Mattoussi − *Department of Chemistry and Biochemistry, Florida State University, Tallahassee, Florida 32306, United States;* orcid.org/0000-0002-6511-9323; Email: mattoussi@fsu.edu

Authors

Wentao Wang − *Department of Chemistry and Biochemistry, Florida State University, Tallahassee, Florida 32306, United States;* orcid.org/0000-0003-2273-4171

Erna A. van Niekerk − *Department of Neurosciences, University of California, San Diego, La Jolla, California 92093, United States*

Yang Zhang − *Laboratory for Molecular Photonics, Department of Chemistry, University of Miami, Coral Gables, Florida 33146, United States;* orcid.org/0000-0003-1011-3001

Liang Du − *Department of Chemistry and Biochemistry, Florida State University, Tallahassee, Florida 32306, United States*

Xin Ji − *Department of Chemistry and Biochemistry, Florida State University, Tallahassee, Florida 32306, United States*

Sisi Wang − *Department of Chemistry and Biochemistry, Florida State University, Tallahassee, Florida 32306, United States*

James D. Baker − *Laboratory for Molecular Photonics, Department of Chemistry, University of Miami, Coral Gables, Florida 33146, United States*

Kimberly Groeniger − *Department of Neurosciences, University of California, San Diego, La Jolla, California 92093, United States*

Françisco M. Raymo − *Laboratory for Molecular Photonics, Department of Chemistry, University of Miami, Coral Gables, Florida 33146, United States;* orcid.org/0000-0002-6163-6606

Complete contact information is available at: https://pubs.acs.org/10.1021/acs.bioconjchem.0c00169

Notes

The raw/processed data required to reproduce these findings cannot be shared at this time as the data also forms part of an ongoing study

The authors declare no competing financial interest.

■ ACKNOWLEDGMENTS

The authors would like to thank FSU and the National Science Foundation (NSF-CHE #1508501), the National Institutes of Health (NIH #R01 DC013080), AFOSR (Grant No. FA9550-18-1-0144), and Kasei-Asahi for financial support. They also would like to thank Banghao Chen and Birong Zeng for the fruitful discussions.

■ REFERENCES

(1) Murray, C. B., Norris, D. J., and Bawendi, M. G. (1993) Synthesis and characterization of nearly monodisperse CdE (E = S, Se, Te) semiconductor nanocrystallites. *J. Am. Chem. Soc. 115*, 8706−8715.

(2) Hines, M. A., and Guyot-Sionnest, P. (1996) Synthesis and characterization of strongly luminescing ZnS-Capped CdSe nanocrystals. *J. Phys. Chem. 100*, 468−471.

(3) Talapin, D. V., Rogach, A. L., Kornowski, A., Haase, M., and Weller, H. (2001) Highly luminescent monodisperse CdSe and CdSe/ZnS nanocrystals synthesized in a hexadecylamine-trioctylphosphine oxide-trioctylphospine mixture. *Nano Lett. 1*, 207−211.

(4) Peng, Z. A., and Peng, X. G. (2001) Formation of high-quality CdTe, CdSe, and CdS nanocrystals using CdO as precursor. *J. Am. Chem. Soc. 123*, 183−184.

(5) Reiss, P., Bleuse, J., and Pron, A. (2002) Highly luminescent CdSe/ZnSe core/shell nanocrystals of low size dispersion. *Nano Lett. 2*, 781−784.

(6) Michalet, X., Pinaud, F., Bentolila, L., Tsay, J., Doose, S., Li, J., Sundaresan, G., Wu, A., Gambhir, S., and Weiss, S. (2005) Quantum dots for live cells, in vivo imaging, and diagnostics. *Science 307*, 538−544.

(7) Medintz, I., Uyeda, H., Goldman, E., and Mattoussi, H. (2005) Quantum dot bioconjugates for imaging, labelling and sensing. *Nat. Mater. 4*, 435−446.

(8) Wegner, K. D., and Hildebrandt, N. (2015) Quantum dots: bright and versatile in vitro and in vivo fluorescence imaging biosensors. *Chem. Soc. Rev. 44*, 4792−4834.

(9) Banerjee, A., Pons, T., Lequeux, N., and Dubertret, B. (2016) Quantum dots−DNA bioconjugates: synthesis to applications. *Interface Focus 6*, 20160064.

(10) Mattoussi, H., Palui, G., and Na, H. B. (2012) Luminescent quantum dots as platforms for probing in vitro and in vivo biological processes. *Adv. Drug Delivery Rev. 64*, 138−166.

(11) Silvi, S., and Credi, A. (2015) Luminescent sensors based on quantum dot-molecule conjugates. *Chem. Soc. Rev. 44*, 4275−4289.

(12) Kairdolf, B. A., Smith, A. M., Stokes, T. H., Wang, M. D., Young, A. N., and Nie, S. M. (2013) Semiconductor Quantum Dots for Bioimaging and Biodiagnostic Applications. *Annu. Rev. Anal. Chem. 6*, 143−162.

(13) Liu, S.-L., Wang, Z.-G., Zhang, Z.-L., and Pang, D.-W. (2016) Tracking single viruses infecting their host cells using quantum dots. *Chem. Soc. Rev. 45*, 1211−1224.

(14) Ji, X., Wang, W., and Mattoussi, H. (2016) Controlling the spectroscopic properties of quantum dots via energy transfer and

charge transfer interactions: Concepts and applications. *Nano Today 11*, 98−121.
(15) Howes, P. D., Chandrawati, R., and Stevens, M. M. (2014) Colloidal nanoparticles as advanced biological sensors. *Science 346*, 1247390−1247310.
(16) Shin, T.-H., and Cheon, J. (2017) Synergism of Nanomaterials with Physical Stimuli for Biology and Medicine. *Acc. Chem. Res. 50*, 567−572.
(17) Chinen, A. B., Guan, C. M., Ferrer, J. R., Barnaby, S. N., Merkel, T. J., and Mirkin, C. A. (2015) Nanoparticle Probes for the Detection of Cancer Biomarkers, Cells, and Tissues by Fluorescence. *Chem. Rev. 115*, 10530−10574.
(18) Zhou, J., Yang, Y., and Zhang, C.-y. (2015) Toward Biocompatible Semiconductor Quantum Dots: From Biosynthesis and Bioconjugation to Biomedical Application. *Chem. Rev. 115*, 11669−11717.
(19) Xu, G., Zeng, S., Zhang, B., Swihart, M. T., Yong, K.-T., and Prasad, P. N. (2016) New Generation Cadmium-Free Quantum Dots for Biophotonics and Nanomedicine. *Chem. Rev. 116*, 12234−12327.
(20) Palui, G., Aldeek, F., Wang, W. T., and Mattoussi, H. (2015) Strategies for interfacing inorganic nanocrystals with biological systems based on polymer-coating. *Chem. Soc. Rev. 44*, 193−227.
(21) Wilhelm, S., Tavares, A. J., Dai, Q., Ohta, S., Audet, J., Dvorak, H. F., and Chan, W. C. W. (2016) Analysis of nanoparticle delivery to tumours. *Nat. Rev. Mater. 1*, 16014.
(22) Mout, R., Moyano, D. F., Rana, S., and Rotello, V. M. (2012) Surface functionalization of nanoparticles for nanomedicine. *Chem. Soc. Rev. 41*, 2539−2544.
(23) Soenen, S. J., Parak, W. J., Rejman, J., and Manshian, B. (2015) (Intra)Cellular Stability of Inorganic Nanoparticles: Effects on Cytotoxicity, Particle Functionality, and Biomedical Applications. *Chem. Rev. 115*, 2109−2135.
(24) Giovanelli, E., Muro, E., Sitbon, G., Hanafi, M., Pons, T., Dubertret, B., and Lequeux, N. (2012) Highly Enhanced Affinity of Multidentate versus Bidentate Zwitterionic Ligands for Long-Term Quantum Dot Bioimaging. *Langmuir 28*, 15177−15184.
(25) Wang, W., Ji, X., Du, L., and Mattoussi, H. (2017) Enhanced Colloidal Stability of Various Gold Nanostructures Using a Multi-coordinating Polymer Coating. *J. Phys. Chem. C 121*, 22901−22913.
(26) Yildiz, I., McCaughan, B., Cruickshank, S. F., Callan, J. F., and Raymo, F. M. (2009) Biocompatible CdSe-ZnS Core-Shell Quantum Dots Coated with Hydrophilic Polythiols. *Langmuir 25*, 7090−7096.
(27) Palui, G., Na, H. B., and Mattoussi, H. (2012) Poly(ethylene glycol)-Based Multidentate Oligomers for Biocompatible Semiconductor and Gold Nanocrystals. *Langmuir 28*, 2761−2772.
(28) Sun, M. H., Yang, L. K., Jose, P., Wang, L., and Zweit, J. (2013) Functionalization of quantum dots with multidentate zwitterionic ligands: impact on cellular interactions and cytotoxicity. *J. Mater. Chem. B 1*, 6137−6146.
(29) Bullen, C., and Mulvaney, P. (2006) The effects of chemisorption on the luminescence of CdSe quantum dots. *Langmuir 22*, 3007−3013.
(30) Aldana, J., Wang, Y. A., and Peng, X. (2001) Photochemical Instability of CdSe Nanocrystals Coated by Hydrophilic Thiols. *J. Am. Chem. Soc. 123*, 8844−8850.
(31) Zhang, F., Lees, E., Amin, F., Gil, P. R., Yang, F., Mulvaney, P., and Parak, W. J. (2011) Polymer-Coated Nanoparticles: A Universal Tool for Biolabelling Experiments. *Small 7*, 3113−3127.
(32) Liu, W. H., Greytak, A. B., Lee, J., Wong, C. R., Park, J., Marshall, L. F., Jiang, W., Curtin, P. N., Ting, A. Y., Nocera, et al. (2010) Compact Biocompatible Quantum Dots via RAFT-Mediated Synthesis of Imidazole-Based Random Copolymer Ligand. *J. Am. Chem. Soc. 132*, 472−483.
(33) Wang, W., Ji, X., Kapur, A., Zhang, C., and Mattoussi, H. (2015) A Multifunctional Polymer Combining the Imidazole and Zwitterion Motifs as a Biocompatible Compact Coating for Quantum Dots. *J. Am. Chem. Soc. 137*, 14158−14172.
(34) Tasso, M., Giovanelli, E., Zala, D., Bouccara, S., Fragola, A., Hanafi, M., Lenkei, Z., Pons, T., and Lequeux, N. (2015) Sulfobetaine−Vinylimidazole Block Copolymers: A Robust Quantum Dot Surface Chemistry Expanding Bioimaging's Horizons. *ACS Nano 9*, 11479−11489.
(35) Zhang, P., Liu, S., Gao, D., Hu, D., Gong, P., Sheng, Z., Deng, J., Ma, Y., and Cai, L. (2012) Click-Functionalized Compact Quantum Dots Protected by Multidentate-Imidazole Ligands: Conjugation-Ready Nanotags for Living-Virus Labeling and Imaging. *J. Am. Chem. Soc. 134*, 8388−8391.
(36) Viswanath, A., Shen, Y., Green, A. N., Tan, R., Greytak, A. B., and Benicewicz, B. C. (2014) Copolymerization and Synthesis of Multiply Binding Histamine Ligands for the Robust Functionalization of Quantum Dots. *Macromolecules 47*, 8137−8144.
(37) Trapiella-Alfonso, L., Pons, T., Lequeux, N., Leleu, L., Grimaldi, J., Tasso, M., Oujagir, E., Seguin, J., d'Orlyé, F., Girard, C., et al. (2018) Clickable-Zwitterionic Copolymer Capped-Quantum Dots for in Vivo Fluorescence Tumor Imaging. *ACS Appl. Mater. Interfaces 10*, 17107−17116.
(38) Dunlap, J. H., Loszko, A. F., Flake, R. A., Huang, Y., Benicewicz, B. C., and Greytak, A. B. (2018) Multiply-Binding Polymeric Imidazole Ligands: Influence of Molecular Weight and Monomer Sequence on Colloidal Quantum Dot Stability. *J. Phys. Chem. C 122*, 26756−26763.
(39) Grazon, C., Chern, M., Ward, K., Lecommandoux, S., Grinstaff, M. W., and Dennis, A. M. (2019) A versatile and accessible polymer coating for functionalizable zwitterionic quantum dots with high DNA grafting efficiency. *Chem. Commun. 55*, 11067−11070.
(40) Medintz, I. L., Clapp, A. R., Mattoussi, H., Goldman, E. R., Fisher, B., and Mauro, J. M. (2003) Self-assembled nanoscale biosensors based on quantum dot FRET donors. *Nat. Mater. 2*, 630−638.
(41) Perng, W., Palui, G., Wang, W., and Mattoussi, H. (2019) Elucidating the Role of Surface Coating in the Promotion or Prevention of Protein Corona around Quantum Dots. *Bioconjugate Chem. 30*, 2469−2480.
(42) Debayle, M., Balloul, E., Dembele, F., Xu, X., Hanafi, M., Ribot, F., Monzel, C., Coppey, M., Fragola, A., Dahan, M., et al. (2019) Zwitterionic polymer ligands: an ideal surface coating to totally suppress protein-nanoparticle corona formation? *Biomaterials 219*, 119357.
(43) Susumu, K., Mei, B. C., and Mattoussi, H. (2009) Multifunctional ligands based on dihydrolipoic acid and polyethylene glycol to promote biocompatibility of quantum dots. *Nat. Protoc. 4*, 424−436.
(44) Susumu, K., Uyeda, H. T., Medintz, I. L., Pons, T., Delehanty, J. B., and Mattoussi, H. (2007) Enhancing the stability and biological functionalities of quantum dots via compact multifunctional ligands. *J. Am. Chem. Soc. 129*, 13987−13996.
(45) Wang, W., Kapur, A., Ji, X., Safi, M., Palui, G., Palomo, V., Dawson, P. E., and Mattoussi, H. (2015) Photoligation of an Amphiphilic Polymer with Mixed Coordination Provides Compact and Reactive Quantum Dots. *J. Am. Chem. Soc. 137*, 5438−5451.
(46) Dahan, M., Levi, S., Luccardini, C., Rostaing, P., Riveau, B., and Triller, A. (2003) Diffusion dynamics of glycine receptors revealed by single-quantum dot tracking. *Science 302*, 442−445.
(47) Cai, E., Ge, P., Lee, S. H., Jeyifous, O., Wang, Y., Liu, Y., Wilson, K. M., Lim, S. J., Baird, M. A., Stone, J. E., et al. (2014) Stable Small Quantum Dots for Synaptic Receptor Tracking on Live Neurons. *Angew. Chem., Int. Ed. 53*, 12484−12488.
(48) Muro, E., Pons, T., Lequeux, N., Fragola, A., Sanson, N., Lenkei, Z., and Dubertret, B. (2010) Small and Stable Sulfobetaine Zwitterionic Quantum Dots for Functional Live-Cell Imaging. *J. Am. Chem. Soc. 132*, 4556−4557.
(49) Park, J., Nam, J., Won, N., Jin, H., Jung, S., Jung, S., Cho, S. H., and Kim, S. (2011) Compact and Stable Quantum Dots with Positive, Negative, or Zwitterionic Surface: Specific Cell Interactions and Non-Specific Adsorptions by the Surface Charges. *Adv. Funct. Mater. 21*, 1558−1566.
(50) Zhan, N. Q., Palui, G., Safi, M., Ji, X., and Mattoussi, H. (2013) Multidentate Zwitterionic Ligands Provide Compact and Highly Biocompatible Quantum Dots. *J. Am. Chem. Soc. 135*, 13786−13795.

https://dx.doi.org/10.1021/acs.bioconjchem.0c00169
Bioconjugate Chem. 2020, 31, 1497−1509

(51) Han, H. S., Martin, J. D., Lee, J., Harris, D. K., Fukumura, D., Jain, R. K., and Bawendi, M. (2013) Spatial charge configuration regulates nanoparticle transport and binding behavior in vivo. *Angew. Chem., Int. Ed. 52*, 1414−1419.
(52) Wang, W., Kapur, A., Ji, X., Zeng, B., Mishra, D., and Mattoussi, H. (2016) Multifunctional and High Affinity Polymer Ligand that Provides Bio-Orthogonal Coating of Quantum Dots. *Bioconjugate Chem. 27*, 2024−2036.
(53) Wang, W., Ji, X., Na, H. B., Safi, M., Smith, A., Palui, G., Perez, J. M., and Mattoussi, H. (2014) Design of a Multi-Dopamine-Modified Polymer Ligand Optimally Suited for Interfacing Magnetic Nanoparticles with Biological Systems. *Langmuir 30*, 6197−6208.
(54) Jin, Z., Du, L., Zhang, C., Sugiyama, Y., Wang, W., Palui, G., Wang, S., and Mattoussi, H. (2019) Modification of Poly(maleic anhydride)-Based Polymers with H2N−R Nucleophiles: Addition or Substitution Reaction? *Bioconjugate Chem. 30*, 871−880.
(55) Palui, G., Avellini, T., Zhan, N., Pan, F., Gray, D., Alabugin, I., and Mattoussi, H. (2012) Photoinduced Phase Transfer of Luminescent Quantum Dots to Polar and Aqueous Media. *J. Am. Chem. Soc. 134*, 16370−16378.
(56) Aldeek, F., Hawkins, D., Palomo, V., Safi, M., Palui, G., Dawson, P. E., Alabugin, I., and Mattoussi, H. (2015) UV and Sunlight Driven Photoligation of Quantum Dots: Understanding the Photochemical Transformation of the Ligands. *J. Am. Chem. Soc. 137*, 2704−2714.
(57) Mattoussi, H., Mauro, J. M., Goldman, E. R., Anderson, G. P., Sundar, V. C., Mikulec, F. V., and Bawendi, M. G. (2000) Self-assembly of CdSe-ZnS quantum dot bioconjugates using an engineered recombinant protein. *J. Am. Chem. Soc. 122*, 12142−12150.
(58) Zeng, B., Palui, G., Zhang, C., Zhan, N., Wang, W., Ji, X., Chen, B., and Mattoussi, H. (2018) Characterization of the Ligand Capping of Hydrophobic CdSe−ZnS Quantum Dots Using NMR Spectroscopy. *Chem. Mater. 30*, 225−238.
(59) Zhang, C., Palui, G., Zeng, B., Zhan, N., Chen, B., and Mattoussi, H. (2018) Non-Invasive Characterization of the Organic Coating of Biocompatible Quantum Dots Using Nuclear Magnetic Resonance Spectroscopy. *Chem. Mater. 30*, 3454−3466.
(60) Hens, Z., and Martins, J. C. (2013) A Solution NMR Toolbox for Characterizing the Surface Chemistry of Colloidal Nanocrystals. *Chem. Mater. 25*, 1211−1221.
(61) Morris, K. F., and Johnson, C. S. (1992) Diffusion-ordered two-dimensional nuclear magnetic resonance spectroscopy. *J. Am. Chem. Soc. 114*, 3139−3141.
(62) Novoa-Carballal, R., Fernandez-Megia, E., Jimenez, C., and Riguera, R. (2011) NMR methods for unravelling the spectra of complex mixtures. *Nat. Prod. Rep. 28*, 78−98.
(63) Stejskal, E. O., and Tanner, J. E. (1965) Spin Diffusion Measurements: Spin Echoes in the Presence of a Time-Dependent Field Gradient. *J. Chem. Phys. 42*, 288−292.
(64) Valentini, M., Vaccaro, A., Rehor, A., Napoli, A., Hubbell, J. A., and Tirelli, N. (2004) Diffusion NMR Spectroscopy for the Characterization of the Size and Interactions of Colloidal Matter: The Case of Vesicles and Nanoparticles. *J. Am. Chem. Soc. 126*, 2142−2147.
(65) Zhang, C., Jin, Z., Zeng, B., Wang, W., Palui, G., and Mattoussi, H. (2020) Characterizing the Brownian Diffusion of Nanocolloids and Molecular Solutions: Diffusion Ordered NMR Spectroscopy versus Dynamic Light Scattering, *J. Phys. Chem. B*, in press. DOI: 10.1021/acs.jpcb.0c02177
(66) Einstein, A. (1905) The motion of elements suspended in static liquids as claimed in the molecular kinetic theory of heat. *Ann. Phys. 17*, 549−560.
(67) Edward, J. T. (1970) Molecular Volumes and Stokes-Einstein Equation. *J. Chem. Educ. 47*, 261.
(68) Mattoussi, H., Cumming, A. W., Murray, C. B., Bawendi, M. G., and Ober, R. (1998) Properties of CdSe nanocrystal dispersions in the dilute regime: Structure and interparticle interactions. *Phys. Rev. B: Condens. Matter Mater. Phys. 58*, 7850−7863.
(69) Dabbousi, B. O., RodriguezViejo, J., Mikulec, F. V., Heine, J. R., Mattoussi, H., Ober, R., Jensen, K. F., and Bawendi, M. G. (1997) (CdSe)ZnS core-shell quantum dots: Synthesis and characterization of a size series of highly luminescent nanocrystallites. *J. Phys. Chem. B 101*, 9463−9475.
(70) Leatherdale, C. A., Woo, W. K., Mikulec, F. V., and Bawendi, M. G. (2002) On the absorption cross section of CdSe nanocrystal quantum dots. *J. Phys. Chem. B 106*, 7619−7622.
(71) Mizuhara, T., Moyano, D. F., and Rotello, V. M. (2016) Using the power of organic synthesis for engineering the interactions of nanoparticles with biological systems. *Nano Today 11*, 31−40.
(72) Alkilany, A. M., Zhu, L., Weller, H., Mews, A., Parak, W. J., Barz, M., and Feliu, N. (2019) Ligand density on nanoparticles: A parameter with critical impact on nanomedicine. *Adv. Drug Delivery Rev. 143*, 22−36.
(73) Debets, M. F., van Berkel, S. S., Dommerholt, J., Dirks, A. J., Rutjes, F. P. J. T., and van Delft, F. L. (2011) Bioconjugation with Strained Alkenes and Alkynes. *Acc. Chem. Res. 44*, 805−815.
(74) Sletten, E. M., and Bertozzi, C. R. (2009) Bioorthogonal Chemistry: Fishing for Selectivity in a Sea of Functionality. *Angew. Chem., Int. Ed. 48*, 6974−6998.
(75) Han, H. S., Devaraj, N. K., Lee, J., Hilderbrand, S. A., Weissleder, R., and Bawendi, M. G. (2010) Development of a Bioorthogonal and Highly Efficient Conjugation Method for Quantum Dots Using Tetrazine-Norbornene Cycloaddition. *J. Am. Chem. Soc. 132*, 7838−7839.
(76) Zhan, N., Palui, G., Merkl, J.-P., and Mattoussi, H. (2016) Bioorthogonal Coupling as a Means of Quantifying the Ligand Density on Hydrophilic Quantum Dots. *J. Am. Chem. Soc. 138*, 3190−3201.
(77) Pons, T., Medintz, I. L., Wang, X., English, D. S., and Mattoussi, H. (2006) Solution-phase single quantum dot fluorescence resonance energy transfer. *J. Am. Chem. Soc. 128*, 15324−15331.
(78) Kononenko, N. L., Claßen, G. A., Kuijpers, M., Puchkov, D., Maritzen, T., Tempes, A., Malik, A. R., Skalecka, A., Bera, S., Jaworski, J., et al. (2017) Retrograde transport of TrkB-containing autophagosomes via the adaptor AP-2 mediates neuronal complexity and prevents neurodegeneration. *Nat. Commun. 8*, 14819.
(79) Rossi, C., Angelucci, A., Costantin, L., Braschi, C., Mazzantini, M., Babbini, F., Fabbri, M. E., Tessarollo, L., Maffei, L., Berardi, N., et al. (2006) Brain-derived neurotrophic factor (BDNF) is required for the enhancement of hippocampal neurogenesis following environmental enrichment. *Eur. J. Neurosci. 24*, 1850−1856.
(80) Park, H., and Poo, M.-m. (2013) Neurotrophin regulation of neural circuit development and function. *Nat. Rev. Neurosci. 14*, 7−23.
(81) Korte, M., Carroll, P., Wolf, E., Brem, G., Thoenen, H., and Bonhoeffer, T. (1995) Hippocampal long-term potentiation is impaired in mice lacking brain-derived neurotrophic factor. *Proc. Natl. Acad. Sci. U. S. A. 92*, 8856−8860.
(82) Lu, P., Blesch, A., Graham, L., Wang, Y., Samara, R., Banos, K., Haringer, V., Havton, L., Weishaupt, N., Bennett, D., et al. (2012) Motor Axonal Regeneration after Partial and Complete Spinal Cord Transection. *J. Neurosci. 32*, 8208−8218.
(83) Zhang, Y., Thapaliya, E. R., Tang, S., Baker, J. D., and Raymo, F. M. (2016) Supramolecular delivery of fluorescent probes in developing embryos. *RSC Adv. 6*, 72756−72760.
(84) Uyeda, H. T., Medintz, I. L., Jaiswal, J. K., Simon, S. M., and Mattoussi, H. (2005) Synthesis of compact multidentate ligands to prepare stable hydrophilic quantum dot fluorophores. *J. Am. Chem. Soc. 127*, 3870−3878.
(85) Spradling, A., and Rubin, G. (1982) Transposition of cloned P elements into Drosophila germ line chromosomes. *Science 218*, 341−347.

https://dx.doi.org/10.1021/acs.bioconjchem.0c00169
Bioconjugate Chem. 2020, 31, 1497−1509